

Chapter 2

World of Nonlinear ODEs

Not only in research, but also in the everyday world... , we would all be better off if more people realized that simple nonlinear systems do not necessarily possess simple dynamic properties.

Robert M. May, mathematical biologist, *Nature*, Vol. 261, 459 (1976)

In the next three chapters some of the more important mathematical properties of nonlinear dynamical systems as well as the diagnostic tools for analyzing such systems will be introduced. This is a vast subject, so we will only present enough so that you can appreciate and understand the various topics that will be presented in subsequent chapters as we explore the various domains of our nonlinear world. Where needed to further our understanding, we will later expand on these nonlinear mathematical concepts, and even introduce some new ones. In this chapter the properties of nonlinear ODE systems are examined, the subsequent two chapters dealing with nonlinear difference equations (commonly referred to as nonlinear *maps*) and, much more briefly, with nonlinear PDEs and cellular automata.

We will begin by discussing the “breakdown” of the linear superposition principle for nonlinear ODEs. Because of this breakdown, many of the “bread and butter” mathematical techniques (such as Laplace transforms and Fourier analysis) for solving linear ODEs no longer work or are useful for attempting to solve nonlinear ODEs. This necessitates the introduction of new mathematical approaches, many of which apply only to certain classes of nonlinear equations. Some of these mathematical methods are beyond the scope and level of this introductory text and will not be covered. Our intention here is to provide a simple, yet sufficient, mathematical framework that the reader can understand and analyze the various nonlinear models that will be presented in ensuing chapters. Our goal is to give you a glimpse of the nonlinear world, not to teach you all the mathematical tricks that exist for solving nonlinear dynamical equations.

It should also be mentioned that the frontiers of nonlinear dynamics are constantly being pushed out with new ideas and applications continually appearing on a regular basis in various research publications. At present there is a somewhat “piecemeal” approach to tackling nonlinear dynamical equations, but, undoubtedly, as the subject matures, new mathematical techniques and concepts will be discovered and further “unification” will occur.

2.1 Breakdown of Linear Superposition

A general feature of all nonlinear dynamical equations, including nonlinear ODEs, is the “breakdown” of linear additivity or superposition. In the nonlinear world, two plus two can sometimes make five and doubling the stimulus may not double the response. In the world of nonlinear dynamics, a linear combination of two solutions to a nonlinear ODE will generally produce a *nonsolution*.

As a simple example of these ideas, let’s look at the amount x of stretching of a spring fixed at one end which has a force F applied to the other. If the force is not too large, a very good approximation to experimental reality is to assume that there is a linear relationship between x and F , viz.,

$$F = kx, \quad (2.1)$$

a relationship which is referred to as *Hooke’s law* after its discoverer Robert Hooke.¹ The positive proportionality constant k is called the *spring constant* and is a measure of the stretchability of the spring.

However, if the applied force is sufficiently large (but not large enough to permanently deform the spring) or if the “spring” is actually is a clever assembly of a collection of springs, Hooke’s law may be inadequate, the relationship between amount of stretching and applied force being nonlinear. For example, if the stretching is symmetric about the equilibrium point, the nonlinear force law

$$F_{NL} = kx + k_2 x^3 \quad (2.2)$$

is often found to be a good approximation to reality.

If the constant $k_2 > 0$, the spring is referred to as a *hard spring* since it is harder to stretch the spring by a given amount x than if only Hooke’s law prevailed ($k_2 = 0$). Doubling the nonlinear force doesn’t double the amount of stretching.

For $k_2 < 0$, the spring is referred to as *soft*. Experimentally, “hard” and “soft spring” situations can be created in the laboratory and many of the nonlinear dynamical properties discussed in this chapter can be verified. The interested reader is referred to Enns and McGuire’s *Nonlinear Physics* ([EM00]) where various simple experimental activities involving hard and soft springs may be found.

Now consider a mass m which is displaced from equilibrium by an amount x and which experiences a restoring force given by $F = -F_{NL}$, no other forces (such as friction) being present. Newton’s second law of motion (force=mass \times acceleration) then yields the following second-order nonlinear ODE for the motion of the mass:

$$m\ddot{x} = F = -kx - k_2 x^3,$$

or, on rearranging and setting $\alpha \equiv k/m$ and $\beta \equiv k_2/m$,

$$\ddot{x} + \alpha x + \beta x^3 = 0. \quad (2.3)$$

¹Although now best remembered for this law, Robert Hooke (1635–1703) was the inventor of the iris diaphragm in cameras, the universal joint in cars, the balance wheel in a watch, and the person who introduced the word “cell” in biology.

If the coefficient $\beta = 0$ (i.e., Hooke's law prevails), this ODE reduces to the well-known linear *simple harmonic oscillator* (SHO) equation,

$$\ddot{x} + \omega^2 x = 0, \quad (2.4)$$

where $\omega = \sqrt{\alpha}$. It is well known that $x_1 = \sin \omega t$ and $x_2 = \cos \omega t$ are independent solutions of the SHO, i.e., substitution of either x_1 or x_2 into the left-hand side (lhs) of the SHO yields 0. An arbitrary linear combination of x_1 and x_2 also yields zero on the lhs, thus confirming the principle of linear superposition.

On the other hand, the linear superposition principle does not hold for the nonlinear ODE (2.3), as shown in the following example.

Example 2-1: Breakdown of Linear Superposition

If x_1 and x_2 are independent solutions of Equation (2.3), show that the linear combination $x_1 + x_2$ doesn't satisfy the equation.

Solution: Since x_1 and x_2 are both solutions of Equation (2.3), then

$$\ddot{x}_1 + \alpha x_1 + \beta x_1^3 = 0, \quad \text{and} \quad \ddot{x}_2 + \alpha x_2 + \beta x_2^3 = 0.$$

Substituting $x_1 + x_2$ into the lhs of (2.3) and using the above relations, we obtain

$$\ddot{x}_1 + \ddot{x}_2 + \alpha(x_1 + x_2) + \beta(x_1 + x_2)^3 = 3\beta x_1 x_2 (x_1 + x_2).$$

At an arbitrary time t , this result is not equal to zero, so the linear combination $x_1 + x_2$ doesn't satisfy the equation, i.e., linear superposition breaks down.

It should be mentioned that for some nonlinear ODEs a *nonlinear superposition* of the solutions may satisfy the original ODE. The form of the nonlinear superposition, however, varies from one nonlinear ODE to the next. An example of nonlinear superposition is left as a problem at the end of the chapter.

As mentioned earlier, with the breakdown of linear superposition it is not too surprising that many of the standard mathematical methods such as Laplace transforms and Fourier series that are used for analytically solving linear ODEs are no longer useful. Specialized techniques (such as those summarized in Daniel Zwillinger's *Handbook of Differential Equations* ([Zwi89])) for obtaining exact analytic solutions exist, but they are not universal, applying to limited classes of nonlinear ODEs, most of which are not of physical interest. Zwillinger's book also outlines methods of obtaining approximate analytical solutions, for example, *perturbation theory* when the nonlinearity is small.

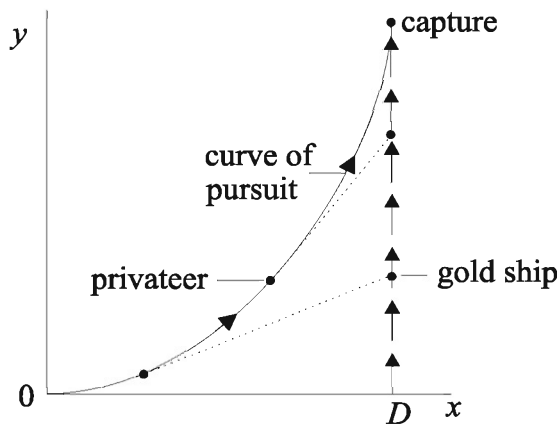
We shall not go into these exact and approximate analytic methods here, being content in the following section to give a few physically interesting examples which can be solved exactly by elementary mathematical techniques. Just because an analytic solution doesn't exist isn't the end of the world. As we shall see in later sections, there exist a host of approaches ranging from phase-plane analysis which can be used to analytically predict *all possible* solutions, to use of the computer to numerically solve *any* nonlinear ODE for given initial or boundary conditions.

2.2 Some Analytically Solvable Examples

According to Harold Davis ([Dav62]), the problem of attempting to determine *curves of pursuit* originated with Leonardo de Vinci but was not really tackled mathematically until the 1700s when the pursuit of heavily laden treasure ships by pirates and privateers² was a problem of much practical interest. In 1732, the French hydrographer Pierre Bouguer (1698–1758) solved the problem of *linear pursuit*, the subject of the following example.

Example 2-2: Linear Pursuit

An English privateer pursues a Spanish gold ship which flees along a straight line. The ratio $r > 1$ of the speeds of the two ships is fixed and the privateer always aims at the gold ship which is initially spotted a distance D km away. The geometry of the linear pursuit problem is summarized in the following figure:



- Derive the nonlinear ODE governing the equation $y(x)$ of the curve of pursuit.
- Analytically solve the ODE for $y(x)$.
- If $r = 2$ and $d = 9$ km, at what value of y does capture take place?

Solution: **a.** The gold ship moves vertically along the line $x = D$. At some instant in time, let the gold ship and privateer coordinates be (D, Y) and (x, y) , respectively. Since the line tangent to the privateer's instantaneous position must pass through the instantaneous position of the gold ship, we have the slope condition

$$\frac{dy}{dx} = \frac{Y - y}{D - x}, \quad \text{or, on rearranging,} \quad Y = (D - x) \frac{dy}{dx} + y. \quad (2.5)$$

The speed of the privateer is r times that of the gold ship. Letting $ds = \sqrt{(dx)^2 + (dy)^2}$

²A privateer was a private warship authorized by a country's government by letters of marque to attack foreign shipping.

be an element of arclength along the curve of pursuit, then $ds/dt = r (dY/dt)$. So,

$$ds = r dY, \quad \text{or,} \quad \sqrt{1 + \left(\frac{dy}{dx}\right)^2} = r \frac{dY}{dx}. \quad (2.6)$$

Differentiating Equation (2.5) with respect to x yields

$$\frac{dY}{dx} = -\frac{dy}{dx} + (D - x) \frac{d^2y}{dx^2} + \frac{dy}{dx} = (D - x) \frac{d^2y}{dx^2}.$$

Substituting this result into the right-hand side (rhs) of (2.6) yields the nonlinear ODE governing the equation of pursuit, viz.,

$$r (D - x) \frac{d^2y}{dx^2} = \sqrt{1 + \left(\frac{dy}{dx}\right)^2}. \quad (2.7)$$

b. To solve the ODE (2.7), we set $p = dy/dx$ and separate variables,

$$\frac{r dp}{\sqrt{1 + p^2}} = \frac{dx}{D - x}.$$

Integrating, we obtain

$$p = \frac{dy}{dx} = \frac{1}{2} \left[\frac{C}{(D - x)^{1/r}} - \frac{(D - x)^{1/r}}{C} \right], \quad (2.8)$$

where C is an arbitrary constant. Integrating a second time yields

$$y = \frac{1}{2} \left[\frac{r C}{(1 - r)} (D - x)^{1-1/r} + \frac{r}{C (1 + r)} (D - x)^{1+1/r} \right] + C', \quad (2.9)$$

where C' is a second arbitrary constant. Since both y and dy/dx are 0 when $x = 0$, then from (2.8) and (2.9), we have $C = D^{1/r}$ and $C' = r D / (r^2 - 1)$. Thus, from (2.9), the curve of pursuit is

$$y = \frac{r D}{(r^2 - 1)} \left[1 + \frac{1}{2} (r - 1) \left(1 - \frac{x}{D}\right)^{1+1/r} - \frac{1}{2} (r + 1) \left(1 - \frac{x}{D}\right)^{1-1/r} \right]. \quad (2.10)$$

c. Capture takes place when $x = D$, in which case $y = r D / (r^2 - 1)$. For $r = 2$ and $D = 9$ km, capture takes place at $y = 6$ km.

A realm of mathematics which is a good source for analytically solvable nonlinear ODEs of physical interest is the so-called *calculus of variations*. The goal of problems in this realm is to determine the function $y(x)$ which maximizes or minimizes an integral I of the form

$$I = \int_a^b F(x, y(x), y'(x)) dx, \quad (2.11)$$

where F is a known integrand and $y' \equiv dy/dx$. The form of $y(x)$ is found by solving the *Euler–Lagrange* equation ([GPS02]),

$$\frac{\partial F}{\partial y} - \frac{d}{dx} \frac{\partial F}{\partial y'} = 0, \quad (2.12)$$

subject to the boundary conditions at the end points a and b .

One of the oldest examples to which this mathematical framework has been applied is the *brachistochrone*³ problem proposed and solved by Johann Bernoulli before posing it to readers of *Acta Eruditorum* in June 1696. The mathematicians Isaac Newton, Jacob Bernoulli (Johann’s brother), Gottfried Leibniz, Ehrenfried Tschirnhaus, and Guillaume de l’Hôpital provided solutions, four (l’Hôpital’s was left out) of which were published in the May 1697 edition of *Acta Eruditorum*.

Example 2-3: The Brachistochrone

Consider the smooth curve $y(x)$ in the following figure joining the origin O ($x = a = 0, y = 0$) and a lower point B ($x = b, y = c$). Starting from rest, a small mass m slides along the curve under the influence of gravity (gravitational acceleration g). What is

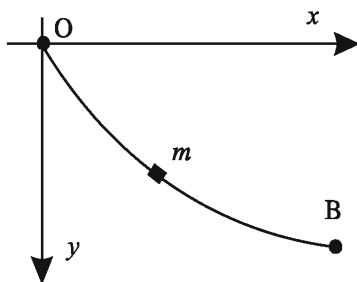


Figure 2.1: Geometry for the brachistochrone.

the equation of the curve which minimizes the time of travel between O and B? Neglect friction.

Solution: If v is the speed of the mass after falling a distance y , then equating the gain in kinetic energy to the decrease in potential energy yields

$$\frac{1}{2} m v^2 = m g y, \quad \text{so} \quad v = \sqrt{2 g y}.$$

If ds is an element of arclength along the curve traced out in the time interval dt , then $v = ds/dt$. Noting that $ds = \sqrt{(dx)^2 + (dy)^2} = \sqrt{1 + (y')^2} dx$, the time for the mass to fall from O to B is

$$T = \int_O^B \frac{ds}{\sqrt{2 g y}} = \int_0^b \left(\frac{1 + (y')^2}{2 g y} \right)^{1/2} dx \equiv \int_0^b F dx. \quad (2.13)$$

³From the Greek: brachisto=shortest, chronos=time.

Substituting F into the Euler–Lagrange equation (2.12), and performing the mathematical operations, yields the nonlinear ODE

$$2y \frac{d^2y}{dx^2} + \left(\frac{dy}{dx} \right)^2 + 1 = 0. \quad (2.14)$$

To solve this ODE, we use the same approach as in the previous example. Setting $p = dy/dx$ and noting that $d^2y/dx^2 = p(dp/dy)$, Equation (2.14) then becomes

$$2yp \frac{dp}{dy} + p^2 + 1 = 0.$$

Integrating, substituting $p = dy/dx$, and separating variables yields

$$dx = \left(\frac{y}{C_1 - y} \right)^{1/2} dy, \quad (2.15)$$

where C_1 is an arbitrary constant. An *implicit solution* $x(y)$ is readily found but it cannot be inverted to give the *explicit solution* $y(x)$. A *parametric solution* may be obtained by introducing the parameter θ through the relation

$$y = \frac{C_1}{2} (1 - \cos \theta) = C_1 \sin^2 \left(\frac{\theta}{2} \right). \quad (2.16)$$

Then (2.15) becomes

$$dx = C_1 \sin^2 \left(\frac{\theta}{2} \right) d\theta,$$

which can be integrated to yield

$$x = \frac{C_1}{2} (\theta - \sin \theta) + C_2, \quad (2.17)$$

where C_2 is a second arbitrary constant. If we choose $\theta = 0$ when $x = 0$, then $C_2 = 0$. Setting $C_1 = 2A$ for convenience, the equations

$$x = A(\theta - \sin \theta), \quad y = A(1 - \cos \theta) \quad (2.18)$$

are just the parametric equations for a *cycloid*, the curve traced out by a point on the rim of a wheel rolling on the x -axis. The curve which minimizes the time of descent from O to B is just a portion of an inverted cycloid. The precise shape depends on the values of b and c which can be used to obtain A .

Both our examples involved answers expressed in terms of elementary functions. The nonlinear spring equation (2.3) with which we began this chapter can also be solved analytically but the answer involves a *special function*, the *Jacobian elliptic function*. Since the mathematics is more involved, we will postpone tackling the nonlinear spring problem until Chapter 5, the *World of Motion*.

2.3 Fixed Points and Phase-Plane Analysis

Consider an ODE system of the so-called *standard* form,

$$\dot{x} = P(x, y), \quad \dot{y} = Q(x, y), \quad (2.19)$$

where P and Q are specified nonlinear functions of x and y . Because P and Q do not depend explicitly on the independent variable t , the system is said to be *autonomous*. Otherwise, it is *nonautonomous*. It should be noted that all ODE systems arising from Newton's second law of mechanics of the structure $\ddot{x} = F(x, \dot{x})$, where F is the force, can be put into the standard form, by setting $\dot{x} = y$, viz.,

$$\dot{x} = y \equiv P, \quad \dot{y} = F(x, y) \equiv Q. \quad (2.20)$$

For example, for the nonlinear spring equation (2.3), one has $Q = -\alpha x - \beta x^3$. Other systems, such as the Lotka–Volterra equations (1.23), are naturally of the standard form. In this case, one can identify $P = ax - bxy$ and $Q = -cy + dxy$.

The *fixed*, or *stationary*, *points* of Equations (2.19) correspond to the points in the x - y plane (the *phase plane*) where $\dot{x} = 0$ and $\dot{y} = 0$. The number and locations of the fixed points in the phase plane are found by solving the simultaneous nonlinear equations

$$P(x, y) = 0, \quad Q(x, y) = 0. \quad (2.21)$$

Unlike the situation for linear ODEs, if P and Q are nonlinear functions, more than one fixed point is possible as illustrated in the following example.

Example 2-4: Rats and Cats

The rat and cat populations on Erehwon evolve with time as follows:

$$\dot{R} = 3R - RC/2, \quad \dot{C} = -C + RC/10.$$

Locate the fixed points of this ODE system.

Solution: Identifying $P(R, C) = R(3 - C/2)$ and $Q(R, C) = C(-1 + R/10)$, there are two fixed points, located at $(R = 0, C = 0)$ and $(R = 10, C = 6)$.

The next step is to determine the behavior of the solution curve, or trajectory, in the vicinity of each fixed point in the phase plane. Since P and Q do not explicitly depend on t , the time can be eliminated by dividing the two equations in (2.19), yielding

$$\frac{dy}{dx} = \frac{Q(x, y)}{P(x, y)}. \quad (2.22)$$

This is just the slope of the trajectory at an arbitrary point (x, y) in the phase plane. At a fixed point, one has $P = Q = 0$, so $dy/dx = 0/0$ and the slope is indeterminate. At any other point (called an *ordinary* point), the slope has a definite unique⁴ value

⁴As a consequence of uniqueness, trajectories cannot cross at ordinary points.

ranging in magnitude from 0 to ∞ . As time advances, the solution will advance along the trajectory determined by the initial values of x and y .

Graphically, one can see **all** possible trajectories of the standard ODE system by creating a *tangent field*. Forming a systematic grid in the phase plane, the ratio $Q(x, y)/P(x, y)$ is calculated at each grid point. A small arrow with slope $dy/dx = Q/P$ is then drawn at each grid point, i.e., tangent to the trajectory at that grid point. The arrowhead should point in the direction of increasing t . Although tangent fields can be drawn by hand, it is recommended (especially if several fixed points are present) that you use a CAS such as *Maple* or *Mathematica* to quickly and accurately do the job.

Example 2-5: Tangent Field

Draw the tangent field for the rats–cats ODE system over the range $R = -5$ to $+15$, $C = -5$ to $+15$. Place small circles at the fixed points. Discuss the possible behavior.

Solution: Let's divide the range in both the R and C directions into 25 equally spaced grid points. The slope $dR/dC = (3R - RC/2)/(-C + RC/10)$ is calculated at each grid point (C, R) . The sense of the arrowheads is determined at each point from the time-dependent ODEs. The resulting tangent field is shown in Figure 2.2. The fixed points at the origin and at $R = 10$, $C = 6$ are represented by the small circles.

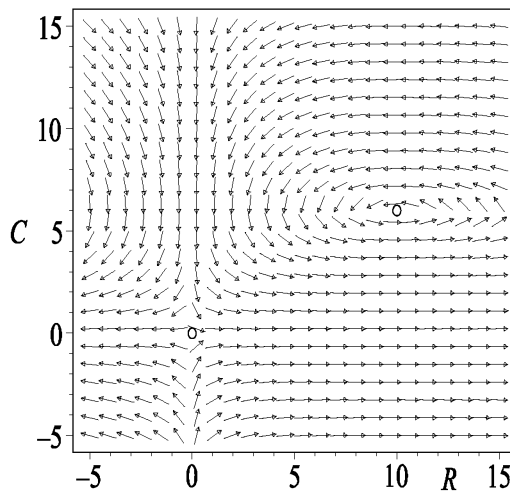


Figure 2.2: Tangent field for the rats–cats ODE system.

Since the rat and cat populations cannot be negative, only the quarter-plane region $R > 0$, $C > 0$ is of physical interest. In this quarter-plane, the tangent field arrows form a counterclockwise “whirlpool” or “vortex” around the fixed point $(R = 10, C = 6)$. For this reason, this fixed point is called a *vortex* point. The behavior of the tangent field arrows tells us that the only possible physical solutions are cyclical.

For the fixed point at the origin, the tangent arrows along the horizontal R axis point away from the fixed point and point toward it along the vertical C axis. This fixed point is an example of a so-called *saddle* point, the name arising from analogy with a saddle point at the pass between two neighboring mountain peaks with two valleys

in the transverse direction. In the mountain situation, increasing height plays the role of increasing time. Using arrows to represent the direction of increasing height, two arrows point away from the mountain saddle point to the two peaks and two arrows point toward the saddle point as one ascends the pass from the valleys.

Let us now turn to the issue of systematically identifying the types of fixed points that are possible and the behavior of the trajectories near each type. We proceed as follows. Let's label the coordinates of a fixed point as (\bar{x}, \bar{y}) . At a nearby ordinary point, the coordinates are $(x = \bar{x} + u, y = \bar{y} + v)$, where u and v are assumed to be small. At this ordinary point, the slope of the trajectory is

$$\frac{dy}{dx} = \frac{Q(\bar{x} + u, \bar{y} + v)}{P(\bar{x} + u, \bar{y} + v)}. \quad (2.23)$$

Since u and v are assumed to be small, the numerator and denominator on the right-hand side of (2.23) can be Taylor expanded about (\bar{x}, \bar{y}) in powers of u and v , so

$$\frac{dy}{dx} = \frac{dv}{du} = \frac{cu + dv + \cdots}{au + bv + \cdots}, \quad (2.24)$$

where

$$a \equiv \left(\frac{\partial P}{\partial x} \right)_{\bar{x}, \bar{y}}, \quad b \equiv \left(\frac{\partial P}{\partial y} \right)_{\bar{x}, \bar{y}}, \quad c \equiv \left(\frac{\partial Q}{\partial x} \right)_{\bar{x}, \bar{y}}, \quad d \equiv \left(\frac{\partial Q}{\partial y} \right)_{\bar{x}, \bar{y}}.$$

Assuming that u and v are sufficiently small, only the linear terms in u and v are retained in (2.24), higher-order terms being neglected. In this case, Equation (2.24) can then be regarded as resulting from the pair of linear ODEs

$$\dot{u} = au + bv, \quad \dot{v} = cu + dv. \quad (2.25)$$

Assuming solutions of the form $(u, v) \sim e^{\lambda t}$, we obtain the two roots

$$\lambda = -\frac{p}{2} \pm \frac{1}{2} \sqrt{p^2 - 4q}, \quad \text{with} \quad p = -(a + d), \quad q = ad - bc.$$

Note that if $q = 0$, the roots are $\lambda = 0$ and $\lambda = -p$. In this case, higher-order terms in the Taylor expansion should be kept. For this reason, $q = 0$ corresponds to a *higher-order fixed point*. The fixed points which occur for $q \neq 0$ are referred to as *simple*. Detailed examination of the roots⁵ for this case reveals that there are only four types of simple fixed points: the *saddle*, *focal* or *spiral*, *nodal*, and *vortex* points. In the neighborhood of these points, the trajectories are as qualitatively depicted in Figure 2.3, the arrows indicating the direction of increasing time. *Stable* focal and nodal points are shown, the trajectories approaching the fixed points as $t \rightarrow +\infty$. For *unstable* focal and nodal points, the arrow directions are reversed.

The ranges of q , p , and $p^2 - 4q$ dictate the type of fixed point and, in the case of the focal and nodal points, its stability. Table 2.1 summarizes all possibilities.

⁵For $p^2 = 4q$, $\lambda = -p/2$. In this degenerate case, a second solution of the form $te^{\lambda t}$ is sought.

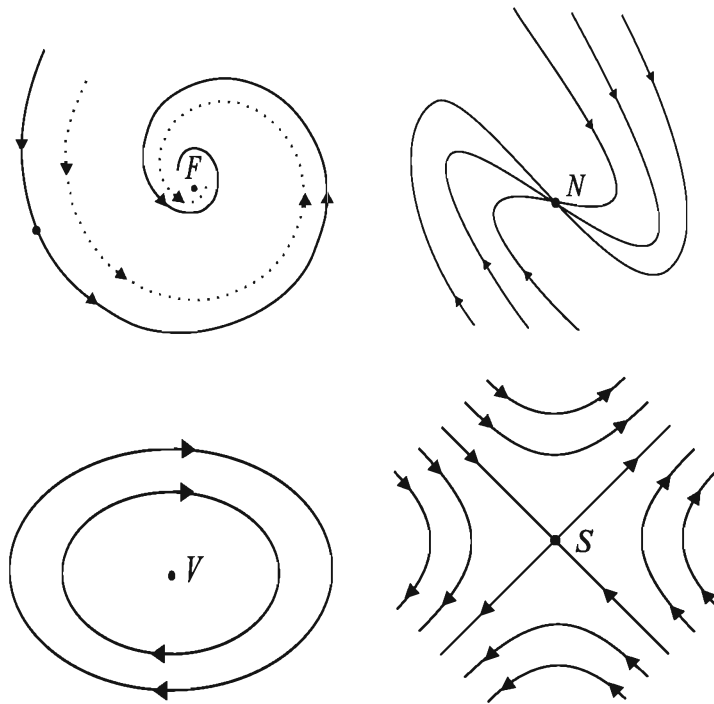


Figure 2.3: Trajectories near a focal (F), nodal (N), vortex (V), saddle (S) point.

Fixed Point	$q = ad - bc$	$p = -(a + d)$	$p^2 - 4q$
saddle	< 0	all p	> 0
higher-order	$= 0$	all p	≥ 0
stable focal	> 0	> 0	< 0
stable nodal		> 0	≥ 0
vortex or focal		$= 0$	< 0
unstable focal		< 0	< 0
unstable nodal		< 0	≥ 0

Table 2.1: Classification of fixed points.

For $q > 0$ and $p = 0$, note that either a vortex or focal point occurs. The “uncertainty” arises because of the neglect of higher-order terms in the Taylor expansion which may turn a closed loop (for the vortex) into a spiral. Although one can examine this situation on a case-by-case basis if desired, the following sufficient, but not necessary, *global* theorem due to Poincaré is often useful:

*If $P(x, -y) = -P(x, y)$ and $Q(x, -y) = Q(x, y)$,
then the fixed point is a vortex, not a focal point.*

Poincaré's theorem is easily proven using symmetry considerations.

The behavior of trajectories near a higher-order fixed point (when $q = 0$) is more complicated. Rather than tackling the issue analytically, a simple way of determining the behavior is to make a *phase-plane portrait* with one or more representative trajectories near the fixed point superimposed on the associated tangent field.

Example 2-6: Phase-Plane Analysis for Rats and Cats

Analytically identify the fixed points of the rats–cats ODE system.

Solution: Recalling that $P(R, C) = R(3 - C/2)$ and $Q(R, C) = C(-1 + R/10)$, the relevant partial derivatives for calculating a , b , c , and d are respectively

$$\partial P/\partial R = 3 - C/2, \quad \partial P/\partial C = -R/2, \quad \partial Q/\partial R = C/10, \quad \partial Q/\partial C = -1 + R/10.$$

For the fixed point at the origin, then $a = 3$, $b = 0$, $c = 0$, and $d = -1$, so that $p = -(a + d) = -2$ and $q = ad - bc = -3$. Since $q < 0$, Table 2.1 tells us that this fixed point is a saddle point. This is consistent with the tangent field shown in Figure 2.2.

For the other fixed point at $(R = 10, C = 6)$, we have $a = 0$, $b = -5$, $c = 6/10$, and $d = 0$. Since $p = -(a + d) = 0$, this fixed point is either a vortex or a focal point. To decide which it is, let's try applying Poincaré's theorem. We find that $P(R, -C) \neq -P(R, C)$ and $Q(R, -C) \neq Q(R, C)$, so the theorem is indecisive.

That the fixed point (probably) is a vortex follows from producing a phase-plane portrait combining a very accurate numerical calculation of the trajectory for a given initial condition with a background of tangent arrows. This is done in Figure 2.4 using

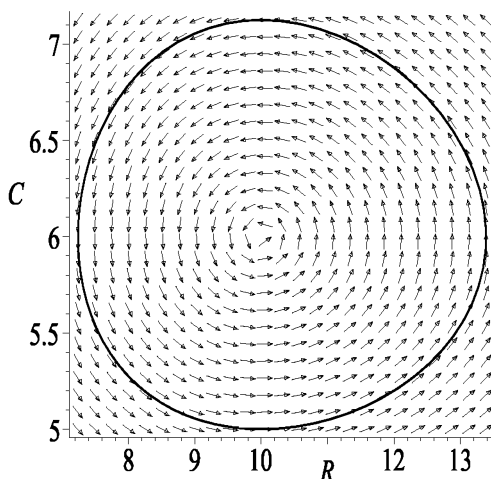


Figure 2.4: Phase-plane portrait for rats and cats.

the adaptive step RKF45 method for the initial condition $R(0) = 10$, $C(0) = 5$. The trajectory is a closed loop about the vortex point at $R = 10$, $C = 6$.

Example 2-7: Higher-Order Fixed Point

Newton's second law of mechanics for the displacement x of a unit mass experiencing a force $F = -x + 2x^2 - x^3$ yields the ODE, $\ddot{x} = -x + 2x^2 - x^3$. Determine the fixed points and produce a phase-plane portrait with a few trajectories and a tangent field. Discuss the result.

Solution: Setting $\dot{x} = y$, the second-order ODE is rewritten in standard form,

$$\dot{x} = y, \quad \dot{y} = -x + 2x^2 - x^3 = -x(1-x)^2.$$

We identify $P = y$ and $Q = -x(1-x)^2$. There are two fixed points, one at $(0,0)$ and a twofold degenerate one at $(1,0)$.

For the fixed point at the origin, $a = 0$, $b = 1$, $c = -1$, and $d = 0$. Then $p = -(a+d) = 0$ and $q = ad - bc = 1 > 0$. From Table 2.1, the fixed point is either a vortex or focal point. Applying Poincaré's theorem,

$$P(x, -y) = -y = -P(x, y), \quad Q(x, -y) = -x(1-x)^2 = Q(x, y).$$

The theorem is satisfied, so the fixed point at the origin is a vortex.

For the degenerate fixed point at $(1,0)$, we have $a = 0$, $b = 1$, $c = 0$, and $d = 0$. Then $p = 0$ and $q = 0$, so this fixed point is a higher-order fixed point.

To see what the topology looks like near this fixed point, a phase-plane portrait is produced with four trajectories corresponding to the initial conditions: $(x(0) = 0, y(0) = 0.35)$, $(-0.4, 0)$, $(-0.1, 0.394)$, and $(-0.1, 0.40)$. With the tangent field included, Figure 2.5 results. The tangent field near the origin and the innermost closed trajectory

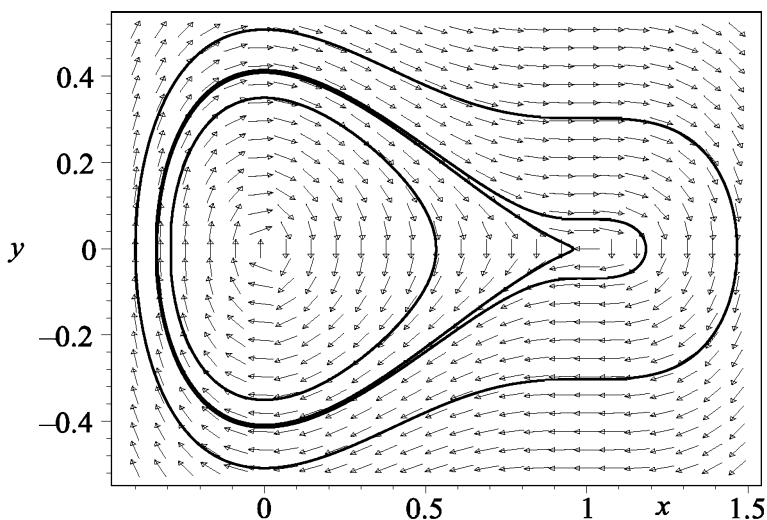


Figure 2.5: Phase-plane portrait for higher-order fixed point.

are consistent with the origin being a vortex. Examining the closest two trajectories to the higher-order fixed point at $(1,0)$, the one to the left of the fixed point is similar to

that near a saddle point, while the one to the right is characteristic of a vortex. The higher-order fixed point looks like the “coalescence” of a saddle and a vortex.

In Problem 1-12 you were asked to numerically determine whether the gnus and sung on the planet Erehwon could coexist together. This question is now answered using phase-plane analysis and creating a phase-plane portrait with a few carefully selected trajectories. The example also introduces you to the concept of *basins of attraction*.

Example 2-8: Only the Lonely

On the bucolic planet of Erehwon, gnus and their backward relatives, the sung, are put together in a large enclosed pasture where they munch on the licorice-flavored clover, their favorite and only food supply. Suppose that the dynamical equations describing the gnu number $g(t)$ and sung number $s(t)$ (per unit area) at time t are

$$\frac{dg}{dt} = g \left(\frac{5}{2} - g \right) - 2gs, \quad \frac{ds}{dt} = s(2 - s) - \frac{3}{2}gs.$$

The first terms in each ODE are Verhulst-like to model the limited food supply available to both species. Since they are after the same food supply, the interaction between the species is detrimental to both, thus both interaction terms have a negative sign.

- Determine the number of fixed points, their locations, and their identity. Use the information to discuss the possible coexistence of the gnus and sung.
- Create a phase-plane portrait which includes the tangent field, trajectories which clearly indicate the possible outcomes as time evolves, and the locations of the fixed points. Use the figure to support your conclusion in part a.

Solution: a. Taking

$$P(g, s) = g \left(\frac{5}{2} - g \right) - 2gs, \quad Q(g, s) = s(2 - s) - \frac{3}{2}gs,$$

and setting them equal to zero yields four fixed points:

$$(g_0, s_0) = (0, 0), (5/2, 0), (0, 2), (3/4, 7/8).$$

The relevant partial derivative for identifying the fixed points are

$$\frac{\partial P}{\partial g} = \frac{5}{2} - 2g - 2s, \quad \frac{\partial P}{\partial s} = -2g, \quad \frac{\partial Q}{\partial g} = -\frac{3}{2}s, \quad \frac{\partial Q}{\partial s} = 2 - 2s - \frac{3}{2}g.$$

Using these partial derivative, the quantities $a, b, c, d, p = -(a + d), q = ad - bc$, and $\Delta \equiv p^2 - 4q$ are evaluated for each fixed point and Table 2.1 used to identify the nature of the fixed point. The results for each fixed point are given in the following table.

So, what can we conclude from the fixed points. The origin is an unstable nodal point, so any initial condition which starts near this point will produce a solution trajectory which moves away from the origin as time evolves. There are two stable nodal

Point	a	b	c	d	p	q	Δ	Type
$(0,0)$	$+\frac{5}{2}$	0	0	$+2$	$-\frac{9}{2}$	$+5$	$\frac{1}{4}$	<i>unstable nodal point</i>
$(\frac{5}{2}, 0)$	$-\frac{5}{2}$	-5	0	$-\frac{7}{4}$	$+\frac{17}{4}$	$+\frac{35}{8}$	$\frac{9}{16}$	<i>stable nodal point</i>
$(0,2)$	$-\frac{3}{2}$	0	-3	-2	$+\frac{7}{2}$	$+3$	$\frac{1}{4}$	<i>stable nodal point</i>
$(\frac{3}{4}, \frac{7}{8})$	$-\frac{3}{4}$	$-\frac{3}{2}$	$-\frac{21}{16}$	$-\frac{7}{8}$	$+\frac{13}{8}$	$-\frac{21}{16}$	$\frac{505}{64}$	<i>saddle point</i>

points which can attract trajectories as $t \rightarrow \infty$. The one at $(g = 5/2, s = 0)$ corresponds to only the gnus surviving, the sung becoming extinct, while the other at $(g = 0, s = 2)$ corresponds to the gnus becoming extinct, the sung being the survivors. Since the fourth fixed point is a saddle point, it appears that the gnus and sung cannot coexist.

b. A phase-plane portrait is now created showing the tangent field, small circles locating the four fixed points, and four trajectories corresponding to the initial conditions, $(g(0), s(0)) = (0.1, 0.15), (0.1, 0.2), (2.5, 2.4), (2.5, 2.5)$. The resulting picture is shown in Figure 2.6. The initial condition $(2.5, 2.5)$ produces a trajectory which heads toward the saddle point at $(3/4, 7/8)$, but suddenly veers upwards in the figure, asymptotically

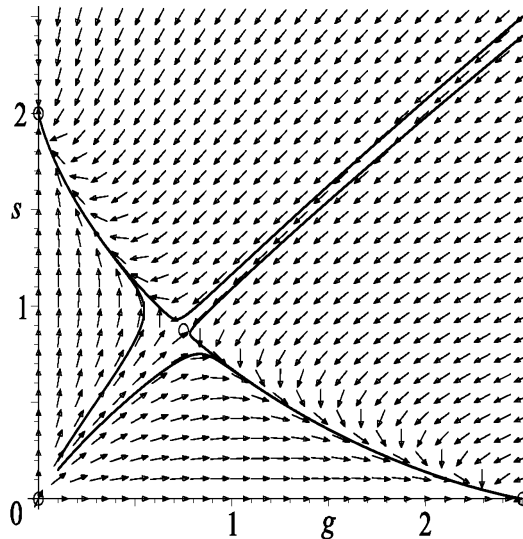


Figure 2.6: Phase-plane portrait for gnus and sung.

approaching the stable nodal point at $(0, 2)$. In this case the gnus become extinct.

Lowering the initial sung population density slightly from 2.5 to 2.4 generates a trajectory which again heads toward the saddle point, but suddenly veers downwards, approaching the other stable nodal point at $(5/2, 0)$. The sung become extinct. We see that the two trajectories approximately divide a portion of the phase plane into *basins of attraction*, the arrows in one basin being attracted to one of the stable nodal points, the arrows in the other basin being attracted to the other stable nodal point.

Similarly, the other two initial conditions, $(0.1, 0.15)$ and $(0.1, 0.2)$, also generate trajectories which approximately divide the remaining portion of the quarter-plane into basins of attraction, each trajectory approaching a different stable nodal point. The dividing lines between the basins are examples of *separatrices*, these lines dividing or separating the phase plane into regions of different behavior. It is this possibility of different outcomes that makes nonlinear ODE systems so interesting.

Putting it all together, unfortunately the gnus and sung cannot coexist.

Combining phase-plane analysis with numerically generated pictures is a very powerful approach to understanding nonlinear ODE systems. The approach can be generalized to systems of three first-order ODEs, but is too involved to present here. See, e.g., Jackson's *Perspectives of Nonlinear Dynamics* ([Jac90]) for the mathematical details.

2.4 Bifurcations

In general, as one or more “control” parameters in a nonlinear ODE model are changed, the location and character of the fixed points change, leading to changes in the topological nature of the possible solution curves. These changes in behavior are referred to as *bifurcations* and the values of the control parameter at which they change are called *bifurcation points*. We will now list and illustrate some⁶ of the more common types of bifurcations that can occur as a single control parameter ε is changed.

a. Saddle-Node Bifurcation: An unstable saddle and a stable node (nodal point) are destroyed (or created) as ε passes through a saddle-node bifurcation point.

Example 2-9: Saddle-Node Bifurcation Point

Show that $\varepsilon = 1$ is a saddle-node bifurcation point for the real nonlinear ODE system

$$\dot{x} = y - 2x, \quad \dot{y} = \varepsilon + x^2 - y.$$

Solution: The fixed points are

$$(\bar{x}, \bar{y}) = (1 + \sqrt{1 - \varepsilon}, 2 + 2\sqrt{1 - \varepsilon}), \quad (1 - \sqrt{1 - \varepsilon}, 2 - 2\sqrt{1 - \varepsilon}),$$

for which

$$p = 3, \quad q = \mp 2\sqrt{1 - \varepsilon}, \quad p^2 - 4q = 9 \pm 8\sqrt{1 - \varepsilon}.$$

⁶For a more complete listing and discussion, see either Verhulst ([Ver90]) or Strogatz ([Str94]).

The upper (lower) sign corresponds to the first (second) fixed point.

Now, consider what happens as ε is increased through $\varepsilon = 1$ from below. For $\varepsilon < 1$, we have $p = 3$ and $q < 0$ for the first fixed point, so it is a saddle. For the second fixed point, $p = 3$, $q > 0$, and $p^2 - 4q > 0$, so it is a stable node.

As $\varepsilon \rightarrow 1$, the two fixed points coalesce into the single degenerate fixed point $(1, 2)$. Since $p = 3$ and $q = 0$, it is a higher-order fixed point.

For $\varepsilon > 1$, there are no real fixed points. The saddle and node are “annihilated” as ε is increased through $\varepsilon = 1$. Conversely, the saddle and node are “born” as the parameter is decreased through the bifurcation point.

b. Transcritical Bifurcation: Two fixed points (e.g., unstable saddle and a stable node) exchange their stability as ε passes through a transcritical bifurcation point.

Example 2-10: Transcritical Bifurcation Point

Show that $\varepsilon = 0$ is a transcritical bifurcation point for the nonlinear system

$$\dot{x} = x(\varepsilon - x), \quad \dot{y} = x - y.$$

Solution: There are two fixed points

$$(\bar{x}, \bar{y}) = (0, 0), \quad (\varepsilon, \varepsilon),$$

for which

$$p = 1 \mp \varepsilon, \quad q = \mp \varepsilon, \quad p^2 - 4q = (\varepsilon \pm 1)^2 \geq 0.$$

The upper (lower) sign applies to the first (second) point.

For $\varepsilon < 0$, we have $q > 0$, $p > 0$, and $p^2 - 4q \geq 0$ for the first fixed point, so it is a stable nodal point. The second fixed point is an unstable saddle point since $q < 0$.

For $\varepsilon > 0$, we have $q < 0$ for the first fixed point so it loses its stability, becoming a saddle. The second fixed point is a stable node, since now $q > 0$, $p > 0$, and $p^2 - 4q \geq 0$. The two fixed points have exchanged their stability as ε passes through 0.

c. Pitchfork Bifurcation: As ε is increased through a pitchfork bifurcation point, a stable fixed point loses its stability, but two other stable fixed points are born. When either of the fixed point coordinates (e.g., x) is plotted versus ε , the stable branches (plotted as solid curves) resemble the handle and two prongs of a pitchfork.

Example 2-11: Pitchfork Bifurcation Point

Show that $\varepsilon = 0$ is a pitchfork bifurcation point for the nonlinear system

$$\dot{x} = x(\varepsilon - x^2), \quad \dot{y} = x - y.$$

Solution: There is a single real fixed point $(0, 0)$ for $\varepsilon < 0$, but three fixed points

$$(\bar{x}, \bar{y}) = (0, 0), \quad (\sqrt{\varepsilon}, \sqrt{\varepsilon}), \quad (-\sqrt{\varepsilon}, -\sqrt{\varepsilon})$$

for $\varepsilon > 0$.

For the fixed point, $(0, 0)$, one has

$$p = 1 - \varepsilon, \quad q = -\varepsilon, \quad p^2 - 4q = (\varepsilon + 1)^2 \geq 0.$$

For $\varepsilon < 0$, then $p > 0$ and $q > 0$, so the fixed point is a stable node. For $\varepsilon > 0$, the fixed point is an unstable saddle since $q < 0$. The fixed point loses its stability as ε is increased through $\varepsilon = 0$.

For both fixed points $(\sqrt{\varepsilon}, \sqrt{\varepsilon})$ and $(-\sqrt{\varepsilon}, -\sqrt{\varepsilon})$, which only exist for $\varepsilon > 0$, we obtain

$$p = 2\varepsilon + 1, \quad q = 2\varepsilon, \quad p^2 - 4q = (2\varepsilon - 1)^2 \geq 0.$$

For $\varepsilon > 0$, one has $p > 0$ and $q > 0$, so they are both stable nodal points. Thus, two symmetrically located stable fixed points are born as ε increases through the critical point $\varepsilon = 0$. If, say, the x -coordinate of the stable fixed points is plotted as a function of ε , the pitchfork shown in Figure 2.7 results.

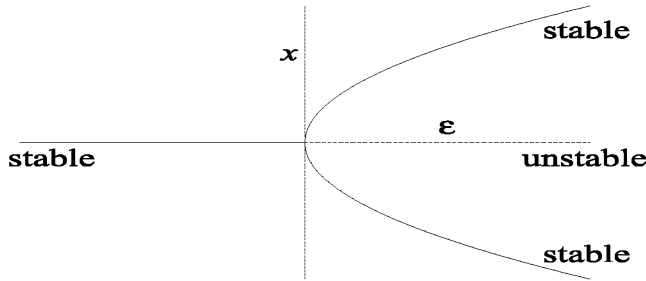


Figure 2.7: Pitchfork bifurcation.

More precisely, this is referred to as a *supercritical* pitchfork bifurcation. A *subcritical* bifurcation occurs at $\varepsilon = 0$ if the term $x(\varepsilon - x^2)$ is replaced with $x(\varepsilon + x^2)$ in the \dot{x} equation. This case is left as a problem.

d. Hopf Bifurcation: A Hopf bifurcation involves the change of stability of a focal or spiral point as the control parameter passes through the bifurcation point.

Example 2-12: Hopf Bifurcation Point

Show that a Hopf bifurcation occurs at $\varepsilon = 0$ for the ODE system

$$\dot{x} = y, \quad \dot{y} = -x + \varepsilon(1 - x^2)y.$$

Solution: The only fixed point is $(0, 0)$, for which $p = -\varepsilon$, $q = 1$, and $p^2 - 4q = \varepsilon^2 - 4$. Since $q > 0$, the origin is a stable focal or nodal point for $\varepsilon < 0$ and an unstable focal or nodal point for $\varepsilon > 0$. For $0 < |\varepsilon| < 2$, it is a focal point since then $p^2 - 4q < 0$. So as ε increases through zero from small negative values, the phase-plane trajectory changes from a stable spiral (spiraling into the origin) to an unstable spiral (spiraling outwards). This is an example of a Hopf bifurcation.

2.5 Hysteresis and the Jump Phenomena

In a typical undergraduate electromagnetism course, students encounter the concept of a *hysteresis* cycle or loop when the flux density B is plotted as a function of the magnetic induction H for a ferromagnet. If H is increased, then decreased, B does not move back down the same curve but, instead, traces out a new path. The reason for this behavior is that the underlying mechanism in a ferromagnet is magnetic domain formation, a process which is nonlinear. As H is decreased, the magnetic domains that are formed are not the same as those when H was increased.

Hysteresis occurs in other contexts (e.g., the current–voltage relation for the superconducting Josephson junction ([Jos62], [Str94]), the Duffing oscillator (introduced shortly)) as well and, as with the ferromagnet, is an indicator that the underlying mechanism is such that the mathematical description is nonlinear. Generally, this mathematics is quite involved so we will be content here to illustrate hysteresis for a simple nonlinear ODE system. This system will also illustrate the so-called *jump phenomena* which are associated with the hysteresis loop that is generated.

Consider the following nonlinear ODE system:

$$\dot{x} = \varepsilon x + 2x^3 - x^5, \quad \dot{y} = x - y, \quad (2.26)$$

with ε a real control parameter which can be varied from negative to positive values.

Setting $\dot{x} = \dot{y} = 0$, it is easy to find the fixed points (\bar{x}, \bar{y}) of this ODE system, as well as determine the ranges for which they are real, and establish their stability. The results are summarized in Table 2.2.

(\bar{x}, \bar{y})	Range	Stability
$(0, 0)$	all ε	$\varepsilon < 0$: stable; $\varepsilon > 0$: unstable
$\pm \left(\sqrt{1 + \sqrt{1 + \varepsilon}}, \sqrt{1 + \sqrt{1 + \varepsilon}} \right)$	$-1 < \varepsilon$	stable
$\pm \left(\sqrt{1 - \sqrt{1 + \varepsilon}}, \sqrt{1 - \sqrt{1 + \varepsilon}} \right)$	$-1 < \varepsilon < 0$	unstable

Table 2.2: Fixed points, ranges for which they are real, and stability.

In a similar manner to what was done for the pitchfork bifurcation in the previous section, let's plot \bar{x} versus ε over a range of ε which includes all the ranges listed in the table, say from $\varepsilon = -2$ to $+2$. The stable branches will be plotted as solid lines, the unstable branches as dotted lines. The curves will further be labeled as stable or unstable for absolute clarity. The resulting picture is shown in Figure 2.8.

For $\varepsilon < -1$, there is only one stable branch, $\bar{x} = 0$. Irrespective of the initial condition, the ODE system will approach the origin as $t \rightarrow +\infty$.

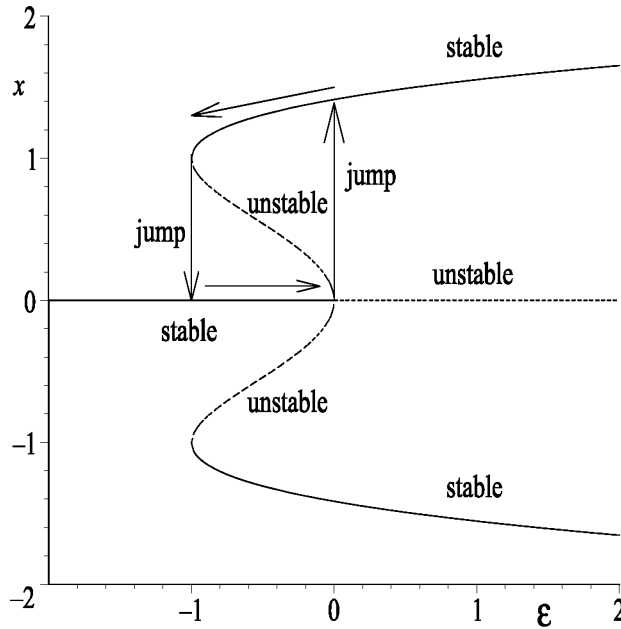


Figure 2.8: Hysteresis loop with jumps.

Now increase ε so that one is in the range $-1 < \varepsilon < 0$. There are three stable branches,

$$\bar{x} = 0, \quad \sqrt{1 + \sqrt{1 + \varepsilon}}, \quad -\sqrt{1 + \sqrt{1 + \varepsilon}},$$

and two unstable branches,

$$\bar{x} = \sqrt{1 - \sqrt{1 + \varepsilon}}, \quad -\sqrt{1 - \sqrt{1 + \varepsilon}}.$$

Which stable branch the system approaches as $t \rightarrow +\infty$ now depends on the choice of initial point. If this point is close to the zero-amplitude branch, the system will evolve toward it, but if it is closer to one of the two non-zero-amplitude branches it will evolve toward the closest of these branches.

Finally, for $\varepsilon > 0$, there are two stable branches, $\bar{x} = \pm \left(\sqrt{1 + \sqrt{1 + \varepsilon}} \right)$, and one unstable branch, $\bar{x} = 0$. Again, which stable branch the system evolves toward depends on the location of the initial point.

So, how does a hysteresis loop occur? Suppose that we start the system in the state $\bar{x} = 0$ for $\varepsilon < -1$ and continuously increase the value of ε . Because this state is stable, the system remains at the origin until $\varepsilon = 0$ is reached at which point the origin loses its stability. Then, the slightest “nudge” will cause the system to “jump” to one of the two non-zero-amplitude branches, e.g., the upper one. Increasing ε further, the system will move to the right along the upper branch. If ε is decreased, the system will remain on the stable upper branch even as ε is decreased through 0. As ε decreases through -1 , the system will jump downwards to the lower stable branch, $\bar{x} = 0$. The hysteresis loop is depicted in Figure 2.8 by arrows with the associated up- and down-jumps indicated.

2.6 Limit Cycles

In considering autonomous nonlinear ODE systems of the standard form ($\dot{x} = P(x, y)$, $\dot{y} = Q(x, y)$, with P and Q nonlinear functions), we have encountered *point attractors* such as the stable focal and nodal points. Another extremely important type of attractor is the stable *limit cycle*, which is an isolated closed trajectory having the property that all other trajectories in its neighborhood wind onto the limit cycle as $t \rightarrow +\infty$.

Why are stable limit cycles important? As we shall see in later chapters, stable limit cycles model systems that display self-sustained oscillations, even in the absence of an external periodic force. The examples range from electronic and chemical oscillators to the beating of the human heart. If the system is perturbed slightly away from a stable limit cycle, it is always attracted back to it.

As a simple mathematical illustration, let's use polar coordinates and consider

$$\dot{r} = r(1 - r), \quad \dot{\theta} = 1, \quad (2.27)$$

where $r \geq 0$ is the radial distance and θ is the angle measured from the positive x -axis of the x - y phase plane. Taking the initial radius and angle to be $r(0) = r_0$ and $\theta(0) = \theta_0$, the ODEs are easily solved. The angular solution is $\theta(t) = t + \theta_0$. Recognizing that the radial equation is just the previously solved logistic ODE, we obtain

$$r(t) = \frac{r_0 e^t}{1 + r_0(e^t - 1)}. \quad (2.28)$$

For any $r_0 < 1$ or $r_0 > 1$, we see that $r(t) \rightarrow 1$ as $t \rightarrow +\infty$. For $r_0 = 1$, then $r(t) = 1$. The circle of radius $r = 1$ is a stable limit cycle. The angular solution tells us that any trajectory starting off the limit cycle will wind onto it in a counterclockwise fashion.

The complete time evolution of a trajectory starting off the limit cycle can be displayed in the x - y phase plane by setting $x = r \cos \theta$ and $y = r \sin \theta$.

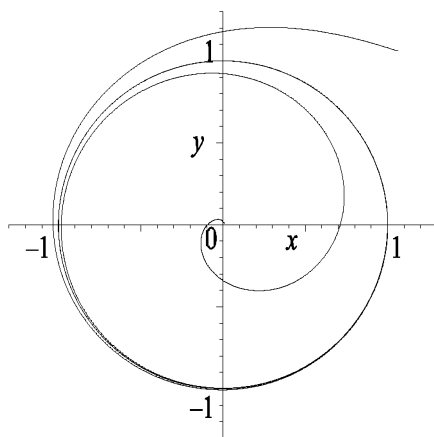


Figure 2.9: Two trajectories approaching the circular limit cycle of radius $r = 1$.

Figure 2.9 shows two trajectories winding onto the stable limit cycle for the two initial radii, $r_0 = 0.01$ and 1.5 , and initial angle $\theta_0 = \pi/4$ radians.

Mathematical models can also be created which display *unstable* and *semistable* limit cycles. For the former, a slight perturbation away from the limit cycle produces trajectories which move away from the limit cycle as $t \rightarrow +\infty$. For the semistable case, trajectories are stable on one side (inside or outside) and unstable on the other. Here's a mathematical example of an unstable limit cycle.

Example 2-13: Unstable Limit Cycle

Consider the nonlinear ODE system

$$\dot{x} = y + x(x^2 + y^2 - 1), \quad \dot{y} = -x + y(x^2 + y^2 - 1).$$

- By converting the system to polar coordinates and analytically solving the resulting equations, show that the system has an unstable limit cycle of radius $r = 1$.
- Plot trajectories over the time range $t = 0$ to 10 for the two initial radii $r_0 = 0.99$ and 1.01 and initial angle $\theta_0 = \pi/4$. Superimpose the tangent field on the plot.

Solution: **a.** Multiplying the \dot{x} equation by x , the \dot{y} equation by y , and adding the resultant equations yields

$$x\dot{x} + y\dot{y} = \frac{1}{2} \frac{d}{dt} (x^2 + y^2) = (x^2 + y^2)(x^2 + y^2 - 1).$$

But $x^2 + y^2 = r^2$, so that this becomes

$$\frac{1}{2} \frac{d}{dt} (r^2) = r\dot{r} = r^2(r^2 - 1), \quad \text{or} \quad \dot{r} = r(r^2 - 1).$$

Separating variables, and integrating with $r(0) = r_0$ at $t = 0$, yields the radial solution

$$r(t) = \frac{r_0}{\sqrt{r_0^2 + (1 - r_0^2)e^{2t}}}.$$

For $r_0 = 1$, $r(t) = 1$ for all t . For $r_0 < 1$, $r(t) \rightarrow 0$ as $t \rightarrow +\infty$. For $r_0 > 1$, $r(t) \rightarrow \infty$ in a *finite* time. The circle of radius 1 is an unstable limit cycle.

The angular sense of the trajectories is found as follows. Multiply the \dot{y} equation by x , the \dot{x} equation by y , and subtract the second equation from the first, again noting that $x^2 + y^2 = r^2$. This yields

$$\dot{\theta} = -1,$$

with the solution

$$\theta(t) = \theta_0 - t.$$

The trajectories wind off the limit cycle in a clockwise sense.

b. The two trajectories winding off the unstable circular limit cycle of radius $r = 1$ are shown in Figure 2.10. Consistent with the tangent field, the inner trajectory winds onto a stable focal point at the origin. The outer trajectory diverges to infinity.

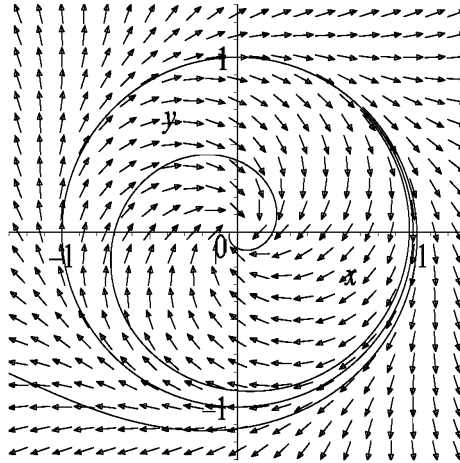


Figure 2.10: Phase-plane portrait for the unstable limit cycle.

A great deal of mathematical effort has gone into deriving general theorems which establish the analytic existence or nonexistence of limit cycles for a given set of nonlinear ODEs of the standard form $\dot{x} = P(x, y)$, $\dot{y} = Q(x, y)$. Two of the more well-known theorems are *Bendixson's negative criterion* and the *Poincaré–Bendixson theorem*.

Bendixson's negative criterion states:

If $\partial P/\partial x + \partial Q/\partial y \neq 0$ doesn't change its sign within a simply connected region of the phase plane, no periodic motions can exist in that region.

A simply connected planar region is one in which any closed curve lying in the region can be shrunk continuously to a point without passing outside the region. That is, a simply connected region has no holes. A proof of this theorem may be found in [EM00].

Example 2-14: Successful Application

Using Bendixson's negative criterion, show that the nonlinear system

$$\dot{x} = -x + y^2, \quad \dot{y} = -y^3 + x^2$$

has no periodic solutions for real x and y , and hence no limit cycles.

Solution: Identifying $P \equiv -x + y^2$ and $Q \equiv -y^3 + x^2$, then

$$\frac{\partial P}{\partial x} + \frac{\partial Q}{\partial y} = -1 - 3y^2,$$

which cannot change sign for real y . So there are no periodic solutions.

The Poincaré–Bendixson theorem states:

Let $x(t)$, $y(t)$ be the parametric equations of a half-trajectory $(0 \leq t < +\infty)$ T which remains inside a finite domain D for $t \rightarrow +\infty$ without approaching any fixed point. Then, either T is itself a closed trajectory or T approaches such a trajectory.

The following example illustrates how this intuitively plausible theorem is applied.

Example 2-15: Existence Proven

Consider the nonlinear system

$$\dot{r} = r(1 - r), \quad \dot{\theta} = 1,$$

with which we began this section. Dividing the first equation by the second eliminates the time, yielding

$$\frac{dr}{d\theta} = r(1 - r).$$

Remembering that the radial coordinate cannot be negative, we have $dr/d\theta > 0$ for $r < 1$ and $dr/d\theta < 0$ for $r > 1$. We also know that $d\theta/dt > 0$.

Let's choose as our domain the annular region D between $r = 0.5$ and $r = 1.5$. There are no fixed points inside this domain or on its boundaries. The trajectories crossing the inner and outer circular boundaries must qualitatively look like those shown in Figure 2.11.

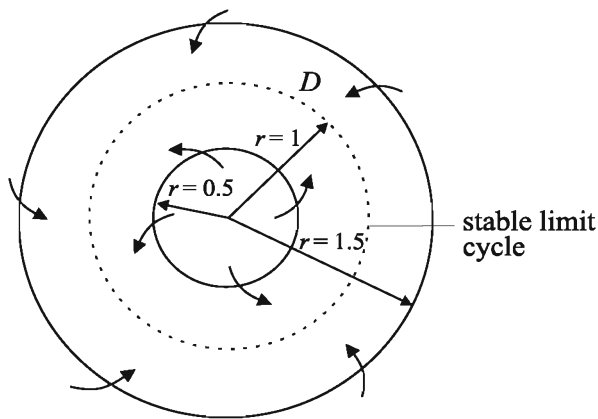


Figure 2.11: Application of the Poincaré–Bendixson theorem.

All the trajectories crossing in through either boundary must be trapped inside the domain, since no arrows leave D . There must exist a half-trajectory that remains inside D as $t \rightarrow \infty$ without approaching any fixed point. So, there is at least one stable limit cycle inside the domain. Of course, we know that there is a circular limit cycle at $r = 1$.

Limit cycles can also occur for autonomous three-dimensional ODE systems. Trying to establish global theorems for the existence or nonexistence of limit cycles in three-dimensional *phase space* is a difficult mathematical task which is beyond the scope of this text. For example, Bendixson's negative criterion doesn't generalize into three dimensions ([Ver90]).

As an example of a three-dimensional ODE system that can display limit cycles, consider the Lorenz model ([Lor63]) equations,⁷

$$\dot{x} = \sigma(y - x), \quad \dot{y} = rx - y - xz, \quad \dot{z} = xy - bz, \quad (2.29)$$

where mathematicians traditionally take $\sigma = 10$, $b = 8/3$, and r as the variable control parameter. Robbins ([Rob79]) and Sparrow ([Spa82]) have explored the bifurcation structure of this system as r is varied.

Sparrow has established ranges of r (e.g., $r = 145$ to 166) where stable limit cycles can occur. Figure 2.12 shows the numerically determined three-dimensional limit cycle

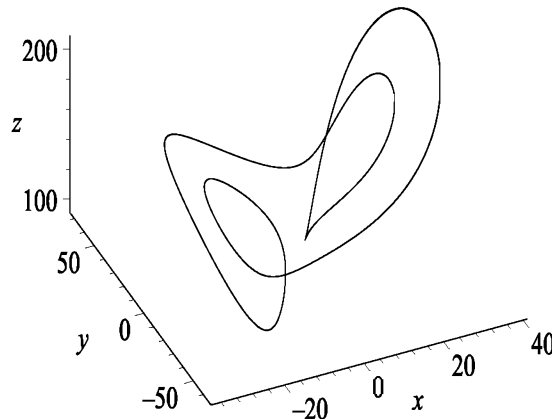


Figure 2.12: Three-dimensional limit cycle for the Lorenz model equations.

over the time range $t = 50$ to 100 for $r = 150$ and $x(0) = 20$, $y(0) = 50$, and $z(0) = 50$. The transient portion $t = 0$ to 50 of the solution curve has been omitted.

2.7 Strange Attractors and Chaos

Three-dimensional systems, such as the Lorenz model, can display still another type of attractor, referred to as a *strange attractor*. For a strange attractor, the solution curve is attracted not to a point or a closed loop, but to a localized region of phase space where

⁷The Lorenz equations arose out of Edward Lorenz's study of atmospheric dynamics. Physically, x is proportional to the convective velocity, y to the temperature difference between ascending and descending flows, and z to the mean convective heat flow. The coefficient σ is the *Prandtl number*, r the reduced *Rayleigh number*, and b is related to the wave number.

it traces out a nonrepeating or *chaotic* path. A strange attractor is characterized by a *fractal*, or noninteger, *dimension*, this concept being discussed shortly. Undoubtedly, the most famous strange attractor is the *butterfly* attractor of the Lorenz system. With σ and b the same as for the above limit cycle, taking $r = 28$ produces the beautiful butterfly strange attractor shown in Figure 2.13. The coordinate axes are omitted.

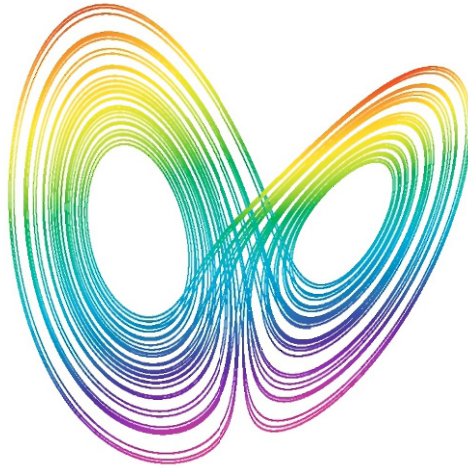


Figure 2.13: Chaotic butterfly strange attractor for the Lorenz system.

Strange attractors can also occur for nonautonomous two-dimensional ODE systems, such as *forced nonlinear oscillators*, because they can be reexpressed as autonomous three-dimensional systems. For example, let's consider the nonlinear mechanical system given by Equation (2.3) which is subjected to an external driving force $F \cos(\omega t)$ as well as a *drag*⁸ force $-2\gamma \dot{x}$. F is the amplitude of the driving force, ω the driving frequency, and γ the damping coefficient. The equation of motion then is *Duffing's equation*,

$$\ddot{x} + 2\gamma \dot{x} + \alpha x + \beta x^3 = F \cos(\omega t). \quad (2.30)$$

Although nonautonomous in two dimensions, Duffing's equation can be recast into an autonomous three-dimensional system by setting $\dot{x} = y$, and $\dot{z} = \omega$ with $z(0) = 0$. Then,

$$\dot{x} = y, \quad \dot{y} = -2\gamma y - \alpha x - \beta x^3 + F \cos z, \quad \dot{z} = \omega. \quad (2.31)$$

To see an example of a strange attractor, let's take⁹

$$\alpha = -1, \quad \beta = 1, \quad \gamma = 0.25, \quad \omega = 1, \quad F = 0.42, \quad \text{and} \quad x(0) = y(0) = 2, \quad z(0) = 0.$$

Because z simply increases linearly with time and is not very interesting, let's plot the trajectory in the x - y phase plane. Taking the time range to be from $t = 0$ to 500 and only plotting the interval $t = 100$ to 500 in order to remove any transient, Figure 2.14 results. The chaotic nature of this localized trajectory, which never approaches a fixed point or

⁸The assumed form (drag force proportional to the velocity) is *Stokes's law of resistance*. Although commonly assumed in elementary physics texts, it is inadequate to describe the motion of many familiar objects such as windmills and helicopter rotors as well as badminton birds and golf balls.

⁹The mathematical case where $\alpha < 0$ and $\beta > 0$ is known as the *inverted Duffing oscillator*.

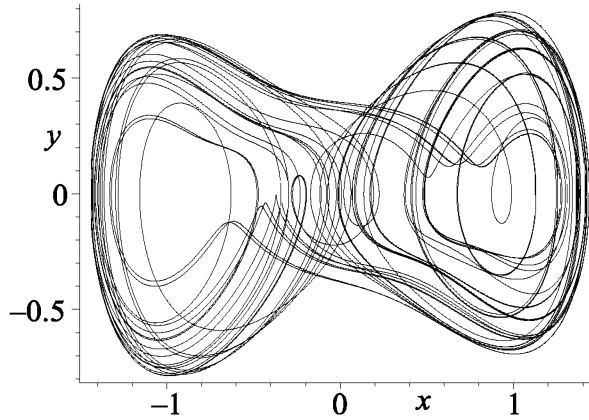
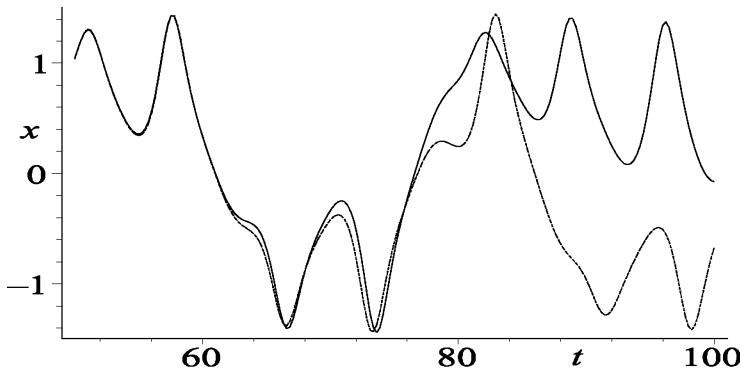


Figure 2.14: Strange attractor for the Duffing oscillator.

a limit cycle, is self-evident. It should be noted that the apparent crossings of the trajectories at ordinary points are an artifact resulting from projecting a 3-dimensional trajectory onto a 2-dimensional plane.

Unlike the situation when periodicity prevails, in the chaotic regime the solution is extremely sensitive to initial conditions, a general feature of nonlinear chaotic models. Figure 2.15 shows $x(t)$ corresponding to the strange attractor in the previous figure as

Figure 2.15: Sensitivity to initial conditions. Solid line: $z(0) = 0$; dashed: $z(0) = 0.001$.

well as the curve obtained by changing $z(0)$ very slightly from 0 to 0.001. Up to about $t = 50$, the solution curves for the two slightly different initial conditions are almost identical but, as seen from the figure, begin to deviate substantially at larger times.

The Lorenz model is a severely truncated version of the full nonlinear PDE system of atmospheric equations. However, the full system is also subject to this same sensitivity to initial conditions. This led Lorenz [Lor63] to conclude that, even for a perfect atmospheric model, the weather cannot be accurately predicted beyond a week or so.

2.8 Fractal Dimensions

Strange attractors are characterized by noninteger, or fractal, dimensions. For the butterfly attractor, for example, Lorenz found ([Lor84]) that it had a fractal dimension of 2.06 ± 0.01 . Since we normally think of dimension taking on integer values, zero for a point, one for a smooth continuous line, two for a smooth continuous surface, and so on, the idea of a noninteger dimension may seem rather strange. It's not! One simply has to generalize the concept of dimension so that it reduces to our familiar cases, but can be used to characterize irregularly shaped lines (e.g., edges of snowflakes, ferns, coastlines, etc.) or lines, surfaces, and volumes (e.g., Swiss cheese) with holes in them.

There are several different ways that the usual concept of dimension can be generalized. We will only discuss the so-called *capacity dimension* D_C . Other types of fractal dimension are discussed in Parker and Chua ([PC89]). Whatever the type, the fractal dimension must reduce to an integer in situations where we would expect it to do so.

To introduce the capacity dimension, let's start by considering a smooth continuous line of length L . Divide the line into equal segments of length $\varepsilon = L/n$, where n is a positive integer (e.g., $n = 3$). Then, the number of segments is $N(\varepsilon) = n = L/\varepsilon$ (e.g., $N = 3 = L/(L/3)$). Now divide each of the n segments into n smaller segments, each of length $\varepsilon = (L/n)/n = L/n^2$. Then, $N(\varepsilon) = n^2 = L/\varepsilon$ (e.g., $N = 3^2 = 9 = L/(L/9)$). Clearly, $N(\varepsilon) = L/\varepsilon$ independent of how many times the subdivision takes place.

Next, consider a smooth continuous square of side L . Divide the square into smaller square boxes, each of length $\varepsilon = L/n$ on a side. The number of boxes to fill the square is $N(\varepsilon) = n^2 = L^2/\varepsilon^2$. If each new box is divided into even smaller boxes of length $\varepsilon = (L/n)/n = L/n^2$ on a side, then the number of boxes is $N(\varepsilon) = n^4 = L^2/\varepsilon^2$. Thus, $N(\varepsilon) = L^2/\varepsilon^2$, no matter how many times the original square is divided.

In three dimensions, the same reasoning leads to $N(\varepsilon) = L^3/\varepsilon^3$, independent of the number of subdivisions. Generalizing to D dimensions, we have $N(\varepsilon) = L^D/\varepsilon^D$. Taking the logarithm of this last expression and solving for D yields

$$D = \frac{\ln N(\varepsilon)}{\ln L + \ln(1/\varepsilon)}.$$

The dependence on the size L may be removed by taking the limit $\varepsilon \rightarrow 0$. Then $\ln(1/\varepsilon) \gg \ln L$, and the capacity dimension is defined as

$$D_C = \lim_{\varepsilon \rightarrow 0} \frac{\ln N(\varepsilon)}{\ln(1/\varepsilon)}. \quad (2.32)$$

This definition is now applied to two examples of nonsmooth lines.

Example 2-16: Cantor Set

Consider a straight line of length $L = 1$. Divide the line into three equal segments and throw away the middle third. Repeat this process for each remaining line segment and determine for each subdivision the number $N(\varepsilon)$ of line segments remaining. Do not count the line segments that are thrown away. Use this result to calculate the capacity dimension D_C of the segmented line with gaps (called a *Cantor set*). Discuss the result.

Solution: Starting with the entire line shown at the top of Figure 2.16, divide the line into three equal parts ($\varepsilon = 1/3$) and throw away the middle segment. The segment

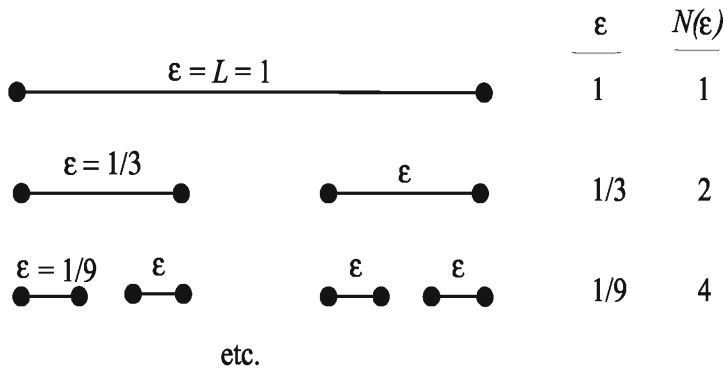


Figure 2.16: The Cantor set.

boundaries are denoted by dots. On this step, the number of remaining line segments is $N(\varepsilon) = 2$. Then divide the remaining two line segments into three equal parts, again throwing away the middle region. Then $\varepsilon = (1/3)^2 = 1/9$ and $N(\varepsilon) = 2^2 = 4$. Generalizing, on the n th step we have $\varepsilon = (1/3)^n$ and $N(\varepsilon) = 2^n$. The capacity dimension is

$$D_c = \lim_{n \rightarrow \infty} (\ln 2^n / \ln 3^n) = \ln 2 / \ln 3 \approx 0.63.$$

The fractal (noninteger) dimension lying between 0 and 1 makes intuitive sense because the resulting line with holes in it is more than a point (zero dimension) but less than a continuous line (one dimension). The Cantor set is an example of a *self-similar* fractal. On each step, the new line segment is a scaled-down version of the old segment.

Example 2-17: Koch Triadic Curve

Consider a line of length 1 unit. Instead of throwing away the middle third as in the Cantor set, form an equilateral triangle in the middle third as shown in Figure 2.17.

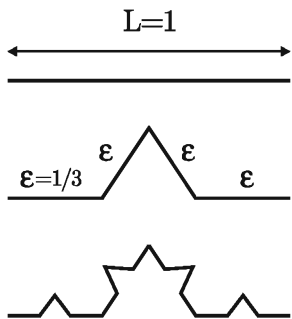


Figure 2.17: The Koch curve.

Each line segment is $\varepsilon = 1/3$. Repeat the process with each new line segment in step 1 to produce step 2. Each line segment now has length $1/9$. Repeating this process indefinitely, determine D_C . Discuss the result.

Solution: On the first step, we have $\varepsilon = 1/3$ and $N(\varepsilon) = 4$. On the second step, $\varepsilon = (1/3)^2 = 1/9$ and $N(\varepsilon) = 4^2 = 16$. Generalizing, on the n th step, $\varepsilon = (1/3)^n$ and $N(\varepsilon) = 4^n$. The capacity dimension is

$$D_C = \lim_{n \rightarrow \infty} (\ln 4^n / \ln 3^n) = \ln 4 / \ln 3 \approx 1.26.$$

The dimension is intermediate to a smooth continuous line (dimension one) and a closed surface (dimension two), so it makes intuitive sense.

In experimental situations, where one doesn't have nice analytical formulas such as in our examples, a *box counting* estimate of the fractal dimension is made. Basically, the object whose fractal dimension is to be determined is covered with a one-, two-, or three-dimensional grid and the number of regions of the grid that are occupied are counted. To obtain a good estimate of D_C , finer and finer grids are taken until it appears that D_C is approaching a limit. For very fine grids, care must be taken to have a sufficient number of experimental points so as to not leave a grid region empty that should actually be occupied. The box counting approach was used by Lorenz in his estimate of the fractal dimension of the butterfly attractor.

2.9 Poincaré Sections

With five parameters and three initial coordinates available, the Duffing oscillator can exhibit a tremendous variation in possible behavior besides the strange attractor. A systematic way of numerically exploring the possible bifurcations is to hold all parameter values fixed except for one, e.g., the force amplitude F , which is allowed to change.

For example, let's vary F from 0.325 to 0.420, holding all other parameter values the same as in the previous subsection. As F is increased, one will observe a sequence of *period doublings* prior to reaching the chaotic attractor at $F = 0.42$. The period of the driving force is $T = 2\pi/\omega$. If the period of the solution (the response) is nT where $n = 1, 2, 3, 4, \dots$, it is referred to as a period-1, period-2, period-3, period-4, etc., solution. The corresponding frequency of the solution is $\omega, \omega/2, \omega/3$, and in general ω/n for period n . The solutions for positive integer $n > 2$ are referred to as *subharmonics*.

A convenient way of graphically viewing the change in periodicity of the solution is to create a *Poincaré section*. One observes the y versus x phase plane at each multiple of the driving period, making sure to eliminate the transient solution. If $n = 1$ (period of solution same as driving period), the solution trajectory will pass through exactly the same point in the phase plane on each complete cycle of the driving force. So the Poincaré section then consists of a single point. For $n = 2$, the solution trajectory will pass through one point in the phase plane on completion of a driving force cycle, and

through a second point on completion of two cycles. This identical pattern will then repeat, so the Poincaré section displays two points. Similarly, period-4 produces four points, and so on. For the strange attractor, a new point is added to the phase plane picture on each cycle, the points however being confined to a localized region.

Returning to the Duffing oscillator, a period-1 solution occurs for $F = 0.325$, period-2 for $F = 0.350$, period-4 for $F = 0.357$, period-8 for $F = 0.358$, the period doubling continuing until the chaotic strange attractor is observed at $F = 0.420$. The Poincaré section, consisting of eight points, is shown on the left of Figure 2.18 for period-8, while the strange attractor is shown on the right.

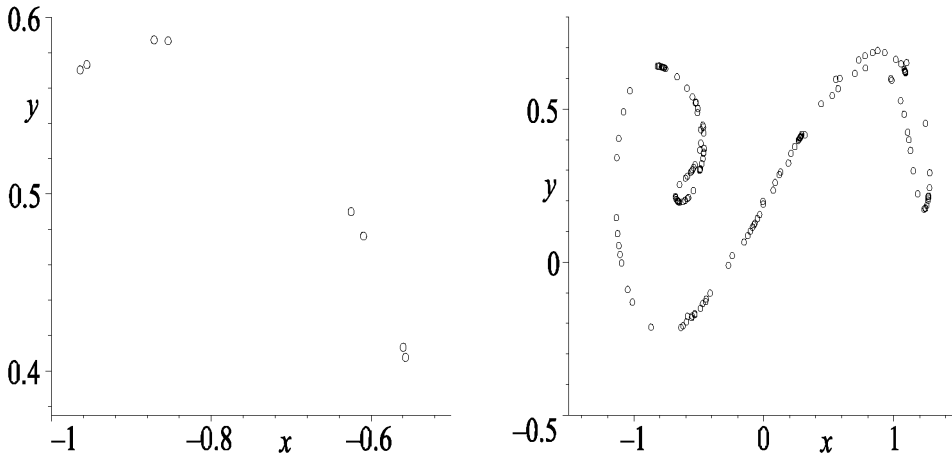


Figure 2.18: Poincaré sections for a (a) period-8 solution, (b) strange attractor.

2.10 Power Spectrum

Another diagnostic tool for studying the change in periodicity or frequency content of the solution $x(t)$ of a time-dependent nonlinear ODE such as Duffing's equation is to calculate the *power spectrum*. Assuming $-\infty < t < +\infty$, the *Fourier transform* $F(\omega)$ of $x(t)$ and its inverse are defined by the following relations:

$$F(\omega) = \int_{-\infty}^{\infty} x(t) e^{-i\omega t} dt, \quad x(t) = \int_{-\infty}^{\infty} F(\omega) e^{i\omega t} d\omega, \quad (2.33)$$

where $i = \sqrt{-1}$. From these definitions, Parseval's theorem, viz.,

$$\int_{-\infty}^{\infty} |x(t)|^2 dt = \int_{-\infty}^{\infty} |F(\omega)|^2 d\omega, \quad (2.34)$$

can be derived. If $x(t)$ is the instantaneous displacement, the left-hand side of (2.34) is proportional to the total energy. Since the right-hand side must have the same dimensions, $|F(\omega)|^2$ represents the energy per unit frequency interval. Aside from a

suitable normalization factor, $S(\omega) \equiv |F(\omega)|^2$ is called the *power spectrum*. It provides information on the distribution of energy as a function of frequency.

For nonlinear ODEs such as the Duffing oscillator, an analytic solution is not possible, so $x(t)$ is not known at every instant in time. A numerical solution must be sought which, because of computational time constraints, only evaluates x at a finite number of discrete time steps. This leads to a number of technical issues (replacing the continuous Fourier transform with the discrete Fourier transform, taking a sufficiently large number of time steps, etc.) in actually calculating $S(\omega)$. These issues are discussed, e.g., in Enns and McGuire ([EM00], [EM01], [EM07]), where *Maple* and *Mathematica* computer recipes for calculating the power spectrum are also provided.

If, for example, all the energy is in a single frequency, the power spectrum will consist of a single vertical “spike” at that frequency. For a period-1 solution, the spike will be at the driving frequency ω . This is illustrated on the left of Figure 2.19 for the Duffing

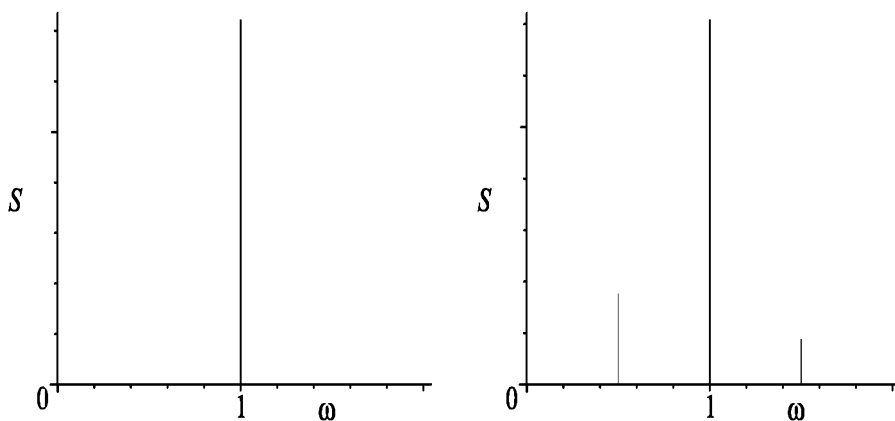


Figure 2.19: Power spectrum for period-1 (left) and period-2 (right).

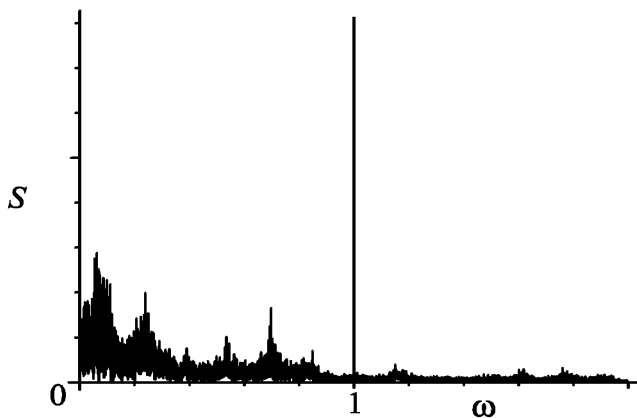


Figure 2.20: Power spectrum for the chaotic Duffing oscillator.

oscillator with $F = 0.325$ and frequency $\omega = 1$ radian/sec, all other parameters the same as in the previous section.

For $F = 0.350$, the power spectrum on the right of the figure results. In addition to the spike at the driving frequency, there is a smaller spike at the *subharmonic* frequency $\omega/2 = 0.5$ rad/sec, indicating that the solution is period-2. Note that there is also a spike in the spectrum at $3(\omega/2) = 1.5$ rad/sec, telling us that there is some energy in the *third harmonic* of the subharmonic frequency. The appearance of harmonics can complicate the power spectrum, but just remember that for period- n , the lowest frequency spike will be at ω/n .

When the solution is chaotic, the corresponding spectrum is spread over all frequencies. An example of such a spectrum, superimposed on the driving frequency spike at $\omega = 1$, is illustrated in Figure 2.20 for $F = 0.420$.

PROBLEMS

Problem 2-1: The Bernoulli ODE

The *Bernoulli* ODE is a first-order nonlinear ODE of the general structure

$$\dot{y} + f_1(t)y = f_2(t)y^n,$$

where n is a constant and f_1 and f_2 are arbitrary functions of t .

Show that the Bernoulli ODE may be reduced to a linear ODE by introducing the new dependent variable

$$z = \frac{1}{y^{n-1}}.$$

A sphere of unit mass falling from rest near the Earth's surface experiences an atmospheric drag force,

$$F_{drag} = -av - bv^2, \quad a > 0, b > 0,$$

where v is the instantaneous speed. Analytically determine $v(t)$.

Problem 2-2: The Riccati ODE

The nonlinear *Riccati* ODE is a first-order nonlinear ODE of the form

$$\dot{y} + ay^2 + f_1(t)y + f_2(t) = 0,$$

where a is a constant and f_1 and f_2 are arbitrary functions of t .

Show that the Riccati ODE may be reduced to a linear ODE by introducing the new dependent variable

$$z = e^a \int_0^t y \, dt.$$

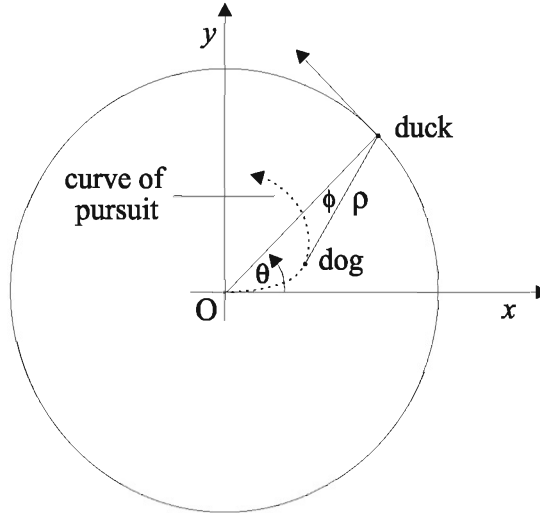
Making use of this result, solve the Riccati ODE for $y(t)$ if

$$f_1(t) = \frac{1}{t}, \quad f_2(t) = \frac{1}{a},$$

being sure to identify the functions which appear in the solution.

Problem 2-3: Circular pursuit

A much more difficult pursuit problem is that of circular pursuit, proposed by A. S. Hathaway ([Hat21]). Referring to the following figure, a dog initially at the center O of a circular pond of unit radius sees a duck swimming counterclockwise along the edge.



Both the dog and the duck swim at constant speed, the ratio of the dog's speed to that of the duck being r .

- a. If the dog always aims at the duck, show that the curve of pursuit is described by the coupled nonlinear ODE system

$$\rho \phi' = \cos \phi - \rho, \quad \rho' = \sin \phi - r,$$

where prime denotes differentiation with respect to θ . This ODE system cannot be analytically solved in closed form.

- b. By numerically determining and plotting the paths traveled by the dog and the duck for some representative values of r , show that the duck eludes capture for $r < 1$ and is caught for $r > 1$.

Problem 2-4: Lane–Emden equation

Consider a spherical cloud of gas of radius R . In equilibrium, the gravitational attraction of the gas molecules is balanced by the pressure p . At a radius $r \leq R$, Newton's law of gravitation tells us that the acceleration g of gravity is

$$g = \frac{G M(r)}{r^2} = -\frac{d\phi}{dr}.$$

G is the gravitational constant, $M(r)$ the mass of cloud inside r , and ϕ the gravitational potential. The decrease in pressure between r and $r + dr$ is

$$dp = -\rho g dr,$$

where ρ is the gas density. Making use of the following assumptions,

- an adiabatic equation of state $p = k \rho^\gamma$ prevails where k is a positive constant and γ is the ratio of specific heat at constant pressure to that at constant volume;
- ϕ satisfies Poisson's equation,

$$\nabla^2 \phi = \frac{d^2 \phi}{dr^2} + \frac{2}{r} \frac{d\phi}{dr} = -4 \pi G \rho;$$

- the boundary conditions are $\phi(R) = \rho(R) = p(R) = 0$ and $\phi(0) = \phi_0$, $g(0) = 0$;

derive the *Lane–Emden* ([Lan70], [Emd07]) nonlinear equation,

$$\frac{d^2 y}{dx^2} + \frac{2}{x} \frac{dy}{dx} + y^n = 0.$$

Here

$$n = \frac{1}{(\gamma - 1)}, \quad y = \frac{\phi}{\phi_0}, \quad x = \sqrt{4 \pi G C \phi_0^{(n-1)}} r, \quad C = \frac{1}{[(n+1)k]^n}.$$

The Lane–Emden equation has analytic solutions for $n = 0, 1, 5$. Derive these solutions. For other n values, the equation must be solved numerically. Solve Emden's equation using the fourth-order Runge–Kutta method for $\gamma = 5/3$ and $\gamma = 7/5$ and plot $y(x)$ for both γ values in the same figure. Discuss the result. What types of gas do the above γ values correspond to?

Problem 2-5: Fixed points of a nonlinear spring

Locate and identify all the fixed points of the nonlinear spring equation,

$$\ddot{x} + \alpha x + \beta x^3 = 0,$$

for the following cases: **(a)** hard spring ($\alpha > 0$, $\beta > 0$); **(b)** soft spring ($\alpha > 0$, $\beta < 0$); **(c)** inverted spring ($\alpha < 0$, $\beta > 0$). Taking $|\alpha| = |\beta| = 1$, plot the tangent field for each case and discuss the possible solution trajectories.

Problem 2-6: Nonlinear superposition for the Riccati ODE

Show that if y_1 , y_2 , and y_3 are solutions of the Riccati equation introduced in Problem 2-2, then y will be a solution if it satisfies

$$\frac{y - y_2}{y - y_1} = C \frac{y_3 - y_2}{y_3 - y_1},$$

where C is an arbitrary constant. ([Zwi89], [Inc64])

Problem 2-7: Multitude of fixed points

Locate and identify the fixed points of the following ODE system (x and y are real and can be positive or negative):

$$\dot{x} = y(1 + x - y^2), \quad \dot{y} = x(1 + y - x^2).$$

Create a phase-plane portrait for this system with the tangent field included and some representative trajectories.

Problem 2-8: Saturable Lotka–Volterra model

To take into account the saturable effect of a large number of prey, the Lotka–Volterra model equations can be extended ([Ver90]) as follows:

$$\dot{x} = ax - b \frac{xy}{1 + sx}, \quad \dot{y} = -cy + d \frac{xy}{1 + sx},$$

where $x, y \geq 0$ are the population numbers (or density) for the prey and predators, respectively, and all coefficients are positive. Discuss the structure of the saturable terms in the model. Determine and identify the fixed points of this system. Use this information and suitable plots to discuss possible solution trajectories.

Problem 2-9: Bifurcation

Determine the type of bifurcation which occurs at the origin for the ODE system

$$\dot{x} = y + \varepsilon x, \quad \dot{y} = -x + \varepsilon y - x^2 y$$

as the control parameter ε passes through 0.

Problem 2-10: Another predator–prey model

Consider the following (dimensionless) predator–prey system ([Ode80]):

$$\dot{x} = x^2(1 - x) - xy, \quad \dot{y} = -\varepsilon y + xy,$$

with $x, y \geq 0$ and $\varepsilon \geq 0$ the control parameter.

- a. Which is the predator and which is the prey?
- b. Locate and identify all the fixed points of this system.
- c. Determine the types of bifurcations which can occur as ε is increased from zero.
- d. Support your analysis with appropriate phase-plane diagrams.

Problem 2-11: Symbiotic interaction

A *symbiotic* interaction between two species is one which is of advantage to both. A simple model ([Mur02]) of symbiosis for two species with normalized population densities x and y is given by the following ODE system:

$$\begin{aligned} \dot{x} &= x(1 - x + ay), \\ \dot{y} &= ry(1 - y + bx), \end{aligned}$$

with the dimensionless parameters a, b , and r all positive. Locate and identify all the physically realizable fixed points of this system. Use the fixed points to qualitatively determine all possible solutions to the ODE system. Confirm your conclusions with supporting tangent field plots.

Problem 2-12: Competing for the same food supply

A simple model ([Mur02]) for two species with normalized population densities x and y competing for the same food supply is given by the following ODE system:

$$\begin{aligned}\dot{x} &= x(1 - x - ay), \\ \dot{y} &= ry(1 - y - bx),\end{aligned}$$

with the dimensionless parameters a , b , and r all positive. Locate and identify all the physically realizable fixed points of this system. Use the fixed points to qualitatively determine all possible solutions to the ODE system. Confirm your conclusions with supporting tangent field plots.

Problem 2-13: Chemostat

A *chemostat* is a device for harvesting bacteria. It consists of a bacterial culture chamber which has an inflow from a nutrient reservoir and an outflow which is adjusted so that the volume of the culture remains constant. In dimensionless form, the governing equations ([EK88]) for the bacterial density N and nutrient concentration C in the chemostat are

$$\begin{aligned}\dot{N} &= \alpha \left(\frac{C}{1+C} \right) N - N, \\ \dot{C} &= - \left(\frac{C}{1+C} \right) N - C + \beta,\end{aligned}$$

where α and β are parameters.

- Determine the fixed points of this nonlinear ODE system. What restrictions must be imposed on α and β so that N and C are never negative?
- Determine the nature of the fixed points and discuss the possible behavior of the system.

Problem 2-14: Baleen whales and krill

Beddington and May ([BM82]) have proposed the following ODE system to model the interaction between baleen whales (population density y) and their main food source, krill (population density x):

$$\begin{aligned}\dot{x} &= rx \left(1 - \frac{x}{K} \right) - axy, \\ \dot{y} &= sy \left(1 - \frac{y}{bx} \right).\end{aligned}$$

Discuss the mathematical structure of this ODE system. Locate and identify all the fixed points.

Problem 2-15: Nested limit cycles

Consider the nonlinear ODE system

$$\begin{aligned}\dot{x} &= -y + x(x^2 + y^2) \sin\left(\frac{1}{\sqrt{x^2 + y^2}}\right), \\ \dot{y} &= x + y(x^2 + y^2) \sin\left(\frac{1}{\sqrt{x^2 + y^2}}\right).\end{aligned}$$

Analytically show that “nested” circular limit cycles of radii $r = 1/(n\pi)$ exist, where $n = 1, 2, 3, \dots$. Show that the limit cycles are stable for even values of n and unstable for odd values.

Problem 2-16: Semistable limit cycle

Analytically show that the nonlinear ODE system

$$\dot{x} = x(x^2 + y^2 - 1)^2 - y, \quad \dot{y} = y(x^2 + y^2 - 1)^2 + x$$

has a semistable limit cycle of radius $r = 1$, stable from the inside and unstable from the outside. Confirm your analysis with a tangent field plot.

Problem 2-17: Circular limit cycle

Consider the second-order nonlinear ODE

$$\ddot{x} + a\dot{x}(x^2 + \dot{x}^2 - 1) + x = 0,$$

with $a > 0$.

- Find and classify all the fixed points.
- Show that the ODE has a circular limit cycle and determine its amplitude, period, and stability.

Problem 2-18: Bendixson’s negative criterion

Use Bendixson’s negative criterion to demonstrate that the following nonlinear ODE systems ([Str94]) have no periodic solutions and, therefore, no limit cycles:

- $\dot{x} = -x + 4y, \quad \dot{y} = -x - y^3;$
- $\dot{x} = -2xe^{(x^2+y^2)}, \quad \dot{y} = -2ye^{(x^2+y^2)};$
- $\dot{x} = y - x^3, \quad \dot{y} = -x - y^3.$

Problem 2-19: Poincaré–Bendixson theorem

Consider the nonlinear ODE system

$$\dot{x} = -x - y + x(x^2 + 2y^2), \quad \dot{y} = x - y + y(x^2 + 2y^2).$$

- Locate and identify all the fixed points.

- b. Reexpress the ODEs in terms of polar coordinates. Choosing appropriate concentric circles of different radii centered on the origin, apply the Poincaré–Bendixson theorem to the annular region to demonstrate that the ODE system has at least one periodic solution.
- c. Make a tangent field plot in the x – y plane which allows you to identify the nature of the periodic solution.

Problem 2-20: Rössler’s strange attractor

By numerically integrating and plotting the solution, show that the 3-dimensional Rössler ODE system ([R76])

$$\dot{x} = -y - z, \quad \dot{y} = x + 0.2y, \quad \dot{z} = 0.2 + (x - \varepsilon)z$$

undergoes a series of period doublings between $\varepsilon = 2.5$ and $\varepsilon = 5.0$, at which point a chaotic strange attractor occurs. Take $x(0) = 4$, $y(0) = 0$, and $z(0) = 0$, and a sufficiently long time in each case to establish the nature of the solution.

Problem 2-21: Koch’s snowflake

Consider an equilateral triangle with sides of unit length. Applying the same procedure as in the Koch triadic curve to each side, determine the capacity dimension of Koch’s *snowflake* curve which results as the procedure is continued indefinitely.

Problem 2-22: Sierpinski’s self-similar fractal gasket

Consider an upright equilateral black triangle with sides of unit length. Remove an inverted equilateral triangle inscribed inside the black triangle with vertex points bisecting the sides of the black triangle. One will now have an inverted white triangular hole with three smaller upright black triangles adjacent to its three sides. Repeat this removal process inside each of the three new black triangles. Repeating the process as many times as necessary and only counting the number of black triangles (i.e., not the white triangular holes), determine the capacity dimension of this geometrical shape, known as Sierpinski’s gasket. Does your answer make intuitive sense? Explain.

Problem 2-23: A non-self-similar fractal

A black square of unit length on each side is divided into nine equal smaller black squares. One of the squares is then selected at random and thrown away, leaving a white square hole in its place. The same process is then applied to the remaining eight black squares, and so on. Counting only the black squares (i.e., not the holes), what is the capacity dimension of this non-self-similar fractal?

Problem 2-24: Modified Cantor set

Instead of removing the middle third as in the Cantor set, remove the middle x fraction from each remaining line segment. Show that the capacity dimension for this modified Cantor set is

$$D_C = \frac{\ln 2}{\ln 2 - \ln(1 - x)}.$$

Explain the limiting cases $x = 0$ and $x = 1$.

Problem 2-25: Poincaré section

Obtain the Poincaré section and determine the Duffing oscillator response for

Pontryagin's maximum principle provides a *necessary condition* to achieve this task. Construct the "Hamiltonian,"

$$H = \psi_1 f_1 + \psi_2 f_2 + \dots + \psi_n f_n + f_0,$$

where the ψ_j are so-called *adjoint variables* which satisfy the adjoint equation,

$$\frac{d\psi_j}{dt} = -\frac{\partial H}{\partial x_j}, \quad j = 1, \dots, n, \quad \left(\text{Note: } \frac{dx_j}{dt} = \frac{\partial H}{\partial \psi_j}, \quad j = 1, \dots, n. \right)$$

For each fixed time t ($0 \leq t \leq T$), choose the control variables $u_j^*(t)$ that maximize the Hamiltonian among all admissible u_j (ψ and x are fixed).

Making use of the Internet, discuss in some detail specific applications of Pontryagin's maximum principle. Here are some examples and the web sites on which they are discussed:

- Minimizing the landing time of a Mars probe; maximizing insect reproduction at the end of the summer season; minimizing the time for a ferry to cross a flowing river; optimal plan for harvesting fish.

<http://www.uccs.edu/rcascava/Math448/PontryaginSP10.pdf>

- Economics problem; optimal harvesting of fish.

<http://www.sjsu.edu/faculty/watkins/pontryag.htm>

- Optimization of the flight phase in ski jumping ([UJ09]).

<http://www.gymnica.upol.cz/index.php/gymnica/article/viewFile/156/143>

- Allocation of energy between growth and reproduction in animal populations ([KT99]).

http://ecology.genebee.msu.ru/3_SOTR/CV_Terekhin_publ/1999_Seasons_EER.pdf

It's a Nonlinear World

Enns, R.H.

2011, XII, 384 p. 145 illus., 8 illus. in color., Hardcover

ISBN: 978-0-387-75338-6